# Solution Structure and Dynamics of the Functional Domain of *Paracoccus denitrificans* Cytochrome $c_{552}$ in Both Redox States[†,‡]

Britta Reincke,[§] Carlos Pérez,[§,||] Primož Pristovšek,[§,⊥] Christian Lücke,[§] Christian Ludwig,[§] Frank Löhr,[§] Vladimir V. Rogov,[§] Bernd Ludwig,[#] and Heinz Rüterjans*[,§]

*Institute of Biophysical Chemistry and Institute of Molecular Genetics, J.W. Goethe−University of Frankfurt, Marie-Curie-Straβe 9, 60439 Frankfurt a.M., Germany*

*Received March 27, 2001; Revised Manuscript Received July 13, 2001*

ABSTRACT: A soluble and fully functional 10.5 kDa fragment of the 18.2 kDa membrane-bound cytochrome $c_{552}$ from *Paracoccus denitrificans* has been heterologously expressed and $^{13}C/^{15}N$-labeled to study the structural features of this protein in both redox states. Well-resolved solution structures of both the reduced and oxidized states have been determined using high-resolution heteronuclear NMR. The overall protein topology consists of two long terminal helices and three shorter helices surrounding the heme moiety. No significant redox-induced structural differences have been observed. $^{15}N$ relaxation rates and heteronuclear NOE values were determined at 500 and 600 MHz. Several residues located around the heme moiety display increased backbone mobility in both oxidation states, while helices I, III, and V as well as the two concatenated $\beta$-turns between Leu30 and Arg36 apparently form a less flexible domain within the protein structure. Major redox-state-dependent differences of the internal backbone mobility on the picosecond−nanosecond time scale were not evident. Hydrogen exchange experiments demonstrated that the slow-exchanging amide proton resonances mainly belong to the helices and $\beta$-turns, corresponding to the regions with high order parameters in the dynamics data. Despite this correlation, the backbone amide protons of the oxidized cytochrome $c_{552}$ exchange considerably faster with the solvent compared to the reduced protein. Using both differential scanning calorimetry as well as temperature-dependent NMR spectroscopy, a significant difference in the thermostabilities of the two redox states has been observed, with transition temperatures of 349.9 K (76.8 °C) for reduced and 307.5 K (34.4 °C) for oxidized cytochrome $c_{552}$. These results suggest a clearly distinct backbone stability between the two oxidation states.

In mitochondria of higher eukaryotes, the electron transfer (ET)[1] between the last two complexes of the respiratory chain, the cytochrome $bc_1$ complex (complex III) and the $aa_3$-type cytochrome *c* oxidase (complex IV), is mediated by a single cytochrome *c* species. These *c*-type cytochromes contain a covalently bound heme moiety, with thioether linkages to the cysteine residues in the conserved Cys-X-Y-Cys-His motif. The heme iron is octahedrally coordinated by the four porphyrin nitrogens and two axial ligands, a histidine and a methionine, and therefore represents a 'low-spin' complex (*1, 2*). During the redox cycle, the iron atom alternates between the diamagnetic reduced (2+) and the paramagnetic oxidized (3+) state.

In bacteria various *c*-type cytochromes are found due to the branching of ET chains, which allows a greater nutritional adaptability and flexibility to environmental demands. *Paracoccus denitrificans* is a Gram-negative facultative anaerobic bacterium found in soil and sewage. Its energy metabolism depends on ET-linked phosphorylation. *P. denitrificans* is an interesting model organism for mitochondrial ET, because of the high sequence homology of its respiratory enzymes with their mitochondrial counterparts. A large number of cytochromes *c*, both soluble and membrane-integrated, have been identified in this bacterium. The membrane-bound 18 kDa cytochrome $c_{552}$, which could be isolated in a "super-complex" with the $bc_1$ complex and the $aa_3$-cytochrome *c* oxidase (*3*), was identified as the genuine electron mediator between complexes III and IV; its deletion or inhibition by a specific antibody suppresses the ET in membranes (*4*). Two soluble fragments of the *P. denitrificans* cytochrome $c_{552}$ have recently been overexpressed in *Escherichia coli*, both lacking the N-terminal membrane anchor domain (*5*). The smaller fragment containing the functional domain, a 10.5 kDa soluble protein of 100 residues, is fully competent in ET to the *P. denitrificans* $aa_3$-oxidase. The expression level of this

[†] This work was supported by Deutsche Forschungsgemeinschaft Grant SFB 472. P.P. was the recipient of a Humboldt fellowship.

[‡] The coordinates of the functional domain of *Paracoccus denitrificans* cytochrome $c_{552}$ in both redox states have been deposited in the RCSB Protein Data Bank under PDB ID codes 1I6D (reduced state) and 1I6E (oxidized state).

* To whom correspondence should be addressed at the Institut für Biophysikalische Chemie, Biozentrum N230 1. OG, Marie-Curie-Strasse 9, 60439 Frankfurt a.M., Germany. Phone: ++49-69-79829631, FAX: ++49-69-79829632, E-mail: hruet@bpc.uni-frankfurt.de.

[§] Institute of Biophysical Chemistry.

[||] Present address: Department of Physical Chemistry, University of Havana, Havana, Cuba.

[⊥] Present address: National Institute of Chemistry, Ljubljana, Slovenia.

[#] Institute of Molecular Genetics.

[1] Abbreviations: DSC, differential scanning calorimetry; ET, electron transfer; HSQC, heteronuclear single-quantum correlation; NOE, nuclear Overhauser effect; NOESY, nuclear Overhauser and exchange spectroscopy; ox., oxidized; *P.*, *Paracoccus*; red., reduced; RMSD, root-mean-square deviation; TOCSY, total correlation spectroscopy.

10.1021/bi010615o CCC: $20.00 
Published on Web 09/20/2001

smaller cytochrome $c_{552}$ fragment (cyt $c_{552}$ hereafter) in *Escherichia coli* is sufficient to allow uniform isotopic labeling.

A large number of cytochrome *c* solution structures have been published [for an overview, see (*6*)], and several comparisons of *c*-type cytochromes in both redox states reported. For *Saccharomyces cerevisae* iso-1-cytochrome *c*, a greater flexibility of the oxidized protein state has been proposed (*7*, *8*), although no significant redox-coupled structural changes could be observed. Based on hydrogen exchange data, a decrease in the number of nonexchanging amide protons, located mainly in the loop regions 14−26 and 75−82, has been detected for the oxidized state by Banci and co-workers. In heteronuclear $^{15}$N relaxation experiments, Fetrow and Baxter found a slightly higher flexibility for the protein in the oxidized state; the loop regions 34−45 and 40−54 were reported as the most flexible on the picosecond−nanosecond time scale in both redox states.

The crystal structure of cyt $c_{552}$ supposedly is more rigid in the reduced state, in particular as the region encompassing residues 40−56 is partially disordered in the oxidized protein (*9*); but in contrast to eukaryotic cytochromes *c* (*10*−*13*), no significant conformational differences could be observed in these high-resolution X-ray structures of cyt $c_{552}$. In this study, we have obtained well-resolved solution structures, investigated the backbone dynamics using $^{15}$N NMR relaxation, performed hydrogen exchange experiments, and determined the thermostability of cyt $c_{552}$ in both redox states, aiming at a better understanding of the molecular interactions and ET mechanisms of cyt $c_{552}$ with its natural redox partners.

## MATERIALS AND METHODS

*Expression and Purification.* The preparation of both nonlabeled and isotope-enriched cyt $c_{552}$ has been described previously (*5*, *14*). Since the oxidized cytochrome cyt $c_{552}$ samples showed protein degradation already after a few days of measurement at room temperature (298 K), they were rechromatographed with a small gel-filtration column after each experiment. The NMR samples were prepared at 1.5−4 mM concentration in argon-purged 20 mM phosphate buffer ($H_2O$:$D_2O$ ratio = 95:5, v/v) at pH 6.0; sodium dithionite and potassium hexacyanoferrate(III) in small excess were used for reduction and oxidation, respectively.

*NMR Data Collection and Processing.* NMR data collection was carried out at 298 K on Bruker DMX spectrometers operating at $^1$H-resonance frequencies of 499.87 and 600.13 MHz using 5 mm triple-resonance ($^1$H/$^{13}$C/$^{15}$N) probes with XYZ-gradient capability. All 3D experiments made use of pulsed field gradients for coherence selection and artifact suppression, and utilized gradient sensitivity enhancement schemes wherever appropriate (*15*, *16*). Homonuclear as well as $^{13}$C- and/or $^{15}$N-edited TOCSY and NOESY experiments (*17*, *18*) were acquired and processed as reported elsewhere (*14*, *19*).

The $^{15}$N relaxation experiments were recorded at two different fields (500 and 600 MHz). Standard sets of sensitivity-enhanced HSQC-type pulse sequences were used to carry out the NMR experiments for the determination of longitudinal ($R_1$) and transverse ($R_2$) relaxation rates as well as the heteronuclear NOE (*20*−*22*). Series of HSQC spectra were recorded in an interleaved mode, each using 8−12 relaxation periods between 2 and 800 ms. The spectral widths were set to 15 ppm/15 ppm in the $^1$H dimension and 38 ppm/35 ppm in the $^{15}$N dimension for reduced/oxidized cyt $c_{552}$, respectively. Echo/antiecho-type gradient selection was used for phase-sensitive detection in the $\omega_1$ dimension. A total of 384 $t_1$ increments were recorded in the indirect dimension, while 1280 data points were recorded in the $t_2$ dimension. The data matrices were Fourier-transformed to 2K × 1K real points using zero filling in both dimensions. Prior to the Fourier transformation, squared sine-bell functions shifted by $\pi/2$ were used for apodization in both dimensions.

For relaxation data analysis, following the measurement of individual signal intensities the relaxation rates were estimated through nonlinear least-squares optimization using the RMX software package (Dr. J. Schmidt, National Institute for Medical Research, London). The resulting relaxation rates $R_1$ and $R_2$ together with the heteronuclear NOE were analyzed by applying a Lipari−Szábo-type model-free formalism using the Modelfree 4.01 software package (*23*, *24*). Paramagnetic effects on the relaxation rates were neglected in the analysis of the oxidized cyt $c_{552}$, since in 'low-spin' systems ($S = 1/2$) these contributions are not significant for protons that do not experience contact shifts and are >7 Å distant from the paramagnetic center (*25*). This is supported by the fact that the relaxation rates in the oxidized state show no observable increase for amide groups close to (<8 Å) the paramagnetic center. Thus, the relaxation data were fitted for each residue to several models of internal dynamics assuming isotropic molecular motion. A grid search was performed using the entire set of experimental data in order to determine the molecular correlation time $\tau_m$.

For the hydrogen exchange experiments, reduced and oxidized samples of nonlabeled cyt $c_{552}$ in 20 mM phosphate buffer (pH 6.0) were lyophilized and subsequently redissolved in $D_2O$ with a small excess of sodium dithionite or potassium hexacyanoferrate(III), respectively. TOCSY experiments were recorded at 298 K on a Bruker DMX 600 spectrometer 1.5 h, 7 h, 13 h, 44.5 h, and 8 days after the exchange.

To investigate the thermostability of cyt $c_{552}$, a number of 1D and 2D NMR spectra were collected on a Bruker DMX 500 spectrometer by raising the temperature stepwise from 298 K, using both reduced (heated to 338 K) and oxidized (heated to 323 K) samples of the nonlabeled protein. Afterward, the samples were slowly returned to 298 K for additional experiments.

*Differential Scanning Calorimetry (DSC) Measurements.* The calorimetric data were recorded using the MC2 scanning microcalorimeter (MicroCal, Northampton, MA) with a heating rate of 45 K/h. The protein samples were equilibrated with buffer containing 5 mM sodium dithionite or potassium hexacyanoferrate(III), to obtain fully reduced or oxidized cyt $c_{552}$, respectively. The molar heat capacities were calculated using the service package 'Origin2.9 for DSC'. Protein specific partial volumes were assumed to be 0.730 $cm^3\ g^{-1}$.

Protein concentrations were determined by the optical densities in solution at 551 nm using an extinction coefficient of 19.4 $mM^{-1}\ cm^{-1}$ ($\Delta\epsilon_{red\text{-}ox}$). The molecular mass of cyt $c_{552}$ was taken as 10.5 kDa.

The molar heat capacity functions, $C_p(T)$, were analyzed as described previously (*26*). For the thermodynamic analysis

of both reduced and oxidized cyt $c_{552}$, a monomolecular "two-state" transition model was chosen.

*Restraints Generation and Structure Calculation.* The NOE-derived distance restraints were determined from 2D homonuclear NOESY and 3D $^{13}$C- or $^{15}$N-edited NOESY−HSQC spectra. Automated assignments of the NOEs, based only on chemical shifts, were obtained with the self-written program *nmr2st*. Peaks that are folded or extremely shifted were assigned manually. Stereospecific assignments of the prochiral methylene and isopropyl methyl groups were obtained using the program GLOMSA (*27*). Pseudo-atom correction for unassigned stereo partners and magnetically equivalent protons was applied as proposed by Wüthrich (*28*).

All structure calculations were performed as described previously for the reduced cyt $c_{552}$ (*6*), with the addition of distance constraints from the $^{13}$C-NOESY spectra. Using the DYANA 1.5 program package (*29*), a total of 100 conformers were calculated in 8000 annealing steps each.

For the paramagnetic oxidized species, experimental pseudocontact shifts were tested as additional structural constraints (*7*, *30*). These calculations were performed with a modified version of the DYANA program called PSEUDYANA (*31*). The tensor parameters for the axial and rhombic anisotropy of the magnetic susceptibility induced by the paramagnetic ion were derived with the program FANTASIA (*32*, *33*) and used as input for the PSEUDYANA calculations.

## RESULTS AND DISCUSSION

The complete resonance assignments of both reduced and oxidized cyt $c_{552}$ have already been reported elsewhere (*14*, *19*) and are available at the BioMagResBank (http://www.bmrb.wisc.edu) under accession numbers BMRB-4471 and BMRB-4777, respectively. The oxidized protein shows less spectral dispersion in the amide region despite the paramagnetic iron center that causes the proton chemical shifts to range from 32.43 ppm (heme HMA) to −33.86 ppm (M78 H$\gamma$). Consequently, triple-resonance experiments on a double-enriched sample were necessary to obtain the sequential resonance assignment of the oxidized protein state. Moreover, the same protein sample was used to obtain a $^{13}$C-NOESY spectrum of reduced cyt $c_{552}$ for further structure refinement with additional distance constraints.

*Chemical Shift Perturbations.* Analogous to reduced cyt $c_{552}$, a number of rather unusual chemical shift values due to ring-current effects were also found in oxidized cyt $c_{552}$. The protons of certain protein residues situated right above or below the heme plane experience considerable upfield shifts away from the standard random coil values (*28*) in both redox states. Furthermore, in the oxidized protein state the paramagnetic iron atom of the heme moiety additionally induces large chemical shift changes for neighboring nuclei. Consequently, the largest redox-state-dependent shifts of proton resonances are thus observed for the heme methyl protons HMA, HMB, HMC, and HMD at 32.43, 13.12, 32.27, and 16.57 ppm, respectively, as well as for the side-chain protons of the two axial ligands to the heme iron.

*Structure Comparison of Cytochrome $c_{552}$ in the Reduced and Oxidized State.* The structural statistics of both reduced and oxidized cyt $c_{552}$ are listed in Table 1. The solution structures of cyt $c_{552}$ in both oxidation states are shown in Figure 1. The overall fold of the protein is basically the same as previously described for the reduced protein (*6*). The structure is tightly packed, consisting of two long α-helices at the N- and C-termini (residues 4−13 and 86−98), three shorter helices (residues 48−53, 59−67, and 69−72) in the middle of the sequence, and several well-defined loop

Table 1: Structural Statistics of the 20 Selected Energy-Minimized Structures of Cytochrome $c_{552}$ from *Paracoccus denitrificans* in Both Redox States[a]

| | reduced | oxidized |
|---|---|---|
| (a) Restraint Statistics | | |
| no. of meaningful NOE distance restraints | 1657 | 1481 |
| intraresidual | 308 | 316 |
| sequential ($\|i-j\|=1$) | 376 | 327 |
| medium range ($1<\|i-j\|<5$) | 358 | 304 |
| long range ($\|i-j\|>4$) | 615 | 534 |
| target function range in DYANA | 0.19−0.34 | 0.14−0.20 |
| no. of violations >0.2 Å | 3 | 3 |
| maximal violation (Å) | 0.27 | 0.28 |
| (b) Structural Precision (Residues 2−99) | | |
| RMSD for Cα atoms (Å) | 0.42 ± 0.09 | 0.41 ± 0.08 |
| RMSD for backbone atoms (Å) | 0.44 ± 0.09 | 0.44 ± 0.07 |
| RMSD for heavy atoms (Å, heme included) | 0.85 ± 0.08 | 0.90 ± 0.08 |
| RMSD with X-ray structure (backbone, Å) | 0.66 ± 0.03 | 0.61 ± 0.03 |
| RMSD with X-ray structure (heavy atoms, Å) | 1.04 ± 0.06 | 1.01 ± 0.04 |
| (c) Ramachandran Plot Quality[b] | | |
| residues in most favored regions (%) | 85.0 | 85.1 |
| residues in additional allowed regions (%) | 14.9 | 14.8 |
| residues in generously allowed regions (%) | 0.1 | 0.1 |
| residues in disallowed regions (%) | 0.1 | 0.0 |

[a] The heme prosthetic group is treated as residue 101. The quality of the structures was evaluated using PROCHECK-NMR (*34*). [b] For nonglycine and nonproline residues.

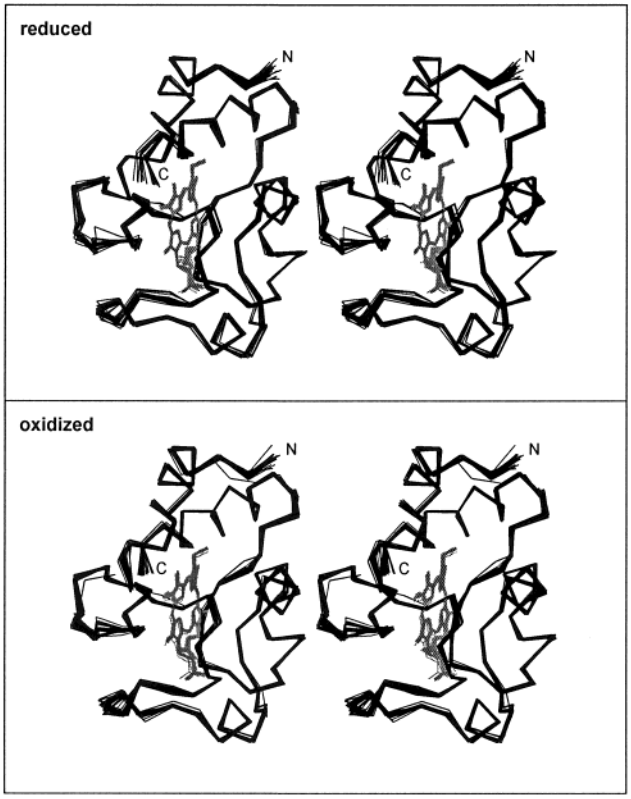


FIGURE 1: Stereoplots showing the ensembles of the 20 final energy-minimized structures of cyt $c_{552}$ in both the reduced (upper panel) and the oxidized state (lower panel). Displayed are the α-carbon traces superposed for residues 2−99. The heme prosthetic group is shown in gray.

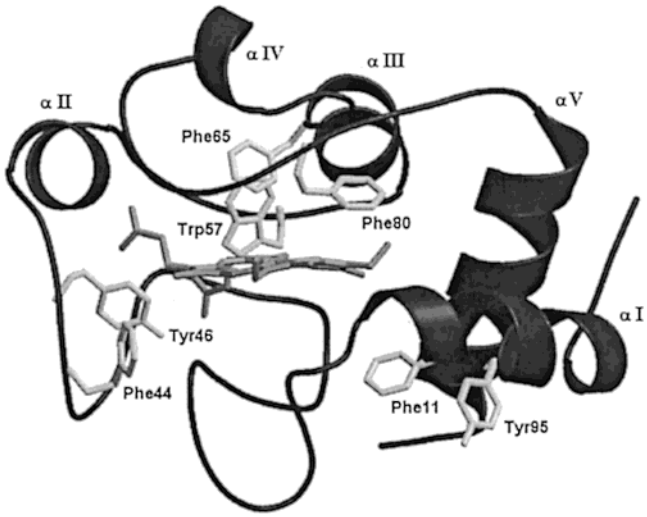


FIGURE 2: Ribbon diagram of cyt $c_{552}$ in the oxidized state. The five α-helices are labeled with Roman numerals. The heme moiety (dark gray) and aromatic rings (light gray) are shown as rods [produced with MOLSCRIPT (*35*) and Raster3D (*36*)].

structures connecting the helices (Figure 2). No significant redox-induced structural differences have been observed between the two energy-minimized structure ensembles. Comparing both ensembles, the backbone and heavy atoms (excluding the terminal residues) show average RMSD values of 0.57 ± 0.07 and 1.01 ± 0.08 Å, respectively. The aromatic phenyl and indole rings are all well-defined, while only the imidazole rings of His29 and His53 display some conformational dispersion. A comparison of the solution structures of cyt $c_{552}$ with the recently determined X-ray structures of the same protein (*9*) also showed no significant differences (see Table 1).

Recently, some minor structural differences regarding the positions of the Trp57 and Phe65 rings had been reported for the solution structure of reduced cyt $c_{552}$ (*6*) relative to the crystal structure (*9*). However, this result could not be reproduced in the course of the present solution structure refinement. The origin of these differences was traced back to erroneous assignments of several aromatic ring protons. Subsequently, we have now corrected these assignments in the BioMagResBank entry BMRB-4471, and the revised structure ensemble of the reduced state has been deposited at the RCSB data bank under PDB ID code 1I6D (replacing the previous entry 1C7M).

Even though the structure ensemble of the oxidized protein state, which is based on NOE data alone, already is of high quality (see Table 1), 152 pseudocontact shift restraints were collected for further structure refinement according to the method described by Banci and co-workers (*7*, *30*). Although the recalculation of the oxidized cyt $c_{552}$ using the PSEUDYANA program package (*31*) did provide a well-defined high-resolution structure ensemble, there was no obvious structural improvement compared to the DYANA results. The ensembles produced with and without pseudocontact shift restraints are virtually identical; the average backbone RMSD between the conformers of both ensembles differs less than 0.05 Å relative to the average backbone RMSD of the conformers within each ensemble. Apparently, the additional information obtained from the $^{15}$N- and in particular $^{13}$C-edited NOESY spectra, which also resulted in a considerable number of stereospecific assignments (113 for the reduced and 115 for the oxidized protein state), already contained sufficient structural data, thus rendering the pseudocontact shift restraint information redundant at least in the present case.

*Backbone Dynamics from $^{15}$N Relaxation Measurements.* The backbone dynamics of cyt $c_{552}$ were studied for both redox states by $^{15}$N relaxation rate ($R_1$ and $R_2$) and steady-state heteronuclear $^{15}$N{$^1$H} NOE measurements at 500 and 600 MHz (Figure 3). The experimental data have been deposited at the BioMagResBank under the accession numbers BMRB-5079 (red.) and BMRB-5080 (ox.). The relaxation rates show similar trends in both reduced and oxidized cyt $c_{552}$. The transverse relaxation rates ($R_2$) are lower in the reduced compared to the oxidized protein (average values approximately 8.5 and 10 s$^{-1}$, respectively). The opposite effect is observed for the longitudinal relaxation rates ($R_1$), which are on average 0.2 s$^{-1}$ higher in the reduced state. These distinctions are due to different molecular correlation times of reduced and oxidized cyt $c_{552}$ ($\tau_m$ = 6.2 and 7.5 ns, respectively). This may be caused by varying sample conditions such as different protein concentrations. On the other hand, an increased partial orientation of the protein in the paramagnetic state as previously observed, e.g., for cytochrome $b_5$ (*37*) could also account for such an effect. Still, the relaxation rate analysis showed that isotropic modeling of the molecular motion is statistically sufficient to describe the dynamic behavior of cyt $c_{552}$ in both oxidation states.

Based on the entire set of experimental relaxation data, the dynamic parameters ($S^2$, $\tau_e$, and $R_{ex}$) have been obtained for the reduced and the oxidized protein (see Supporting Information). According to the order parameter ($S^2$) values, the backbone mobility of cyt $c_{552}$ on the picosecond−nanosecond time scale is very similar in both redox states (Figure 4), with average $S^2$ values of reduced and oxidized cyt $c_{552}$ at 0.857 ± 0.056 and 0.887 ± 0.061, respectively. The residues Gly25, Gly43, Tyr46, Lys74, and Phe80 show strongly decreased order parameters in both oxidation states, with $S^2$ values < 0.79 and 0.82 (more than one standard deviation below the average) for the reduced and the oxidized protein, respectively. Furthermore, several other residues also exhibit order parameter values significantly below average in both oxidation states ($0.79 < S^2 < 0.84$ for reduced and $0.82 < S^2 < 0.87$ for oxidized cyt $c_{552}$), as shown in Figure 5a. Two residues represent borderline cases: Gly55, which falls into the lowest $S^2$ category in the reduced state but only into the second lowest category in the oxidized state; and Gly82, which behaves vice versa. These more flexible parts of the protein backbone are all located around the heme moiety (see Figure 5a) with distances to the heme iron mostly above 8 Å, thus excluding paramagnetic effects on the $^{15}$N relaxation behavior (*8*) except possibly for the amide protons of Cys17 (7.1 Å), His18 (6.2 Å), Gly27 (6.6 Å), Met78 (6.8 Å), Ala79 (6.4 Å), and Phe80 (6.9 Å). However, none of the latter residues shows any observable increase of the relaxation rates in the paramagnetic protein state. Only Phe80 does show a significant effect in the order parameter value. A major influence of the paramagnetic center on the Phe80 amide group relaxation behavior can be ruled out though, since this decrease in $S^2$ occurs in both redox states (see Figure 4).

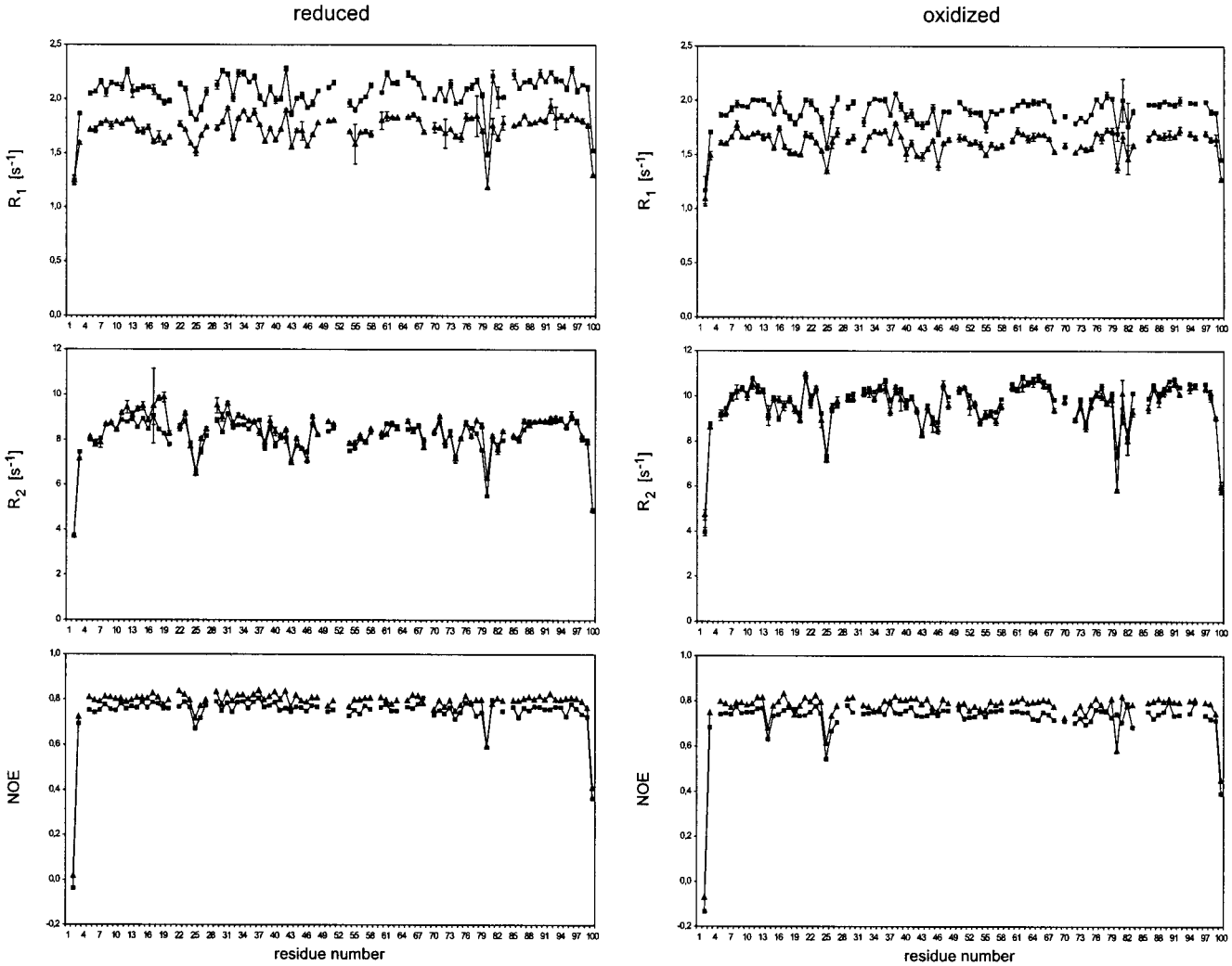


FIGURE 3: Line plots showing the experimental $R_1$, $R_2$, and heteronuclear NOE values at 600 (▲) and 500 (■) MHz for reduced (left panels) and oxidized (right panels) cyt $c_{552}$. The error bars for the NOE have been omitted, as they were set to a constant value (0.03) for all residues.

The decreased order parameter value obtained for Gly82 in the oxidized state might be of interest in the discussion about the cyt $c_{552}$ unfolding process. As reported for iso-1-cytochrome *c* from *Saccharomyces cerevisiae* in the oxidized state (*7*), the region encompassing residues 70−85 (corresponding to 68−83 in cyt $c_{552}$) may be involved in the early unfolding steps. Even though helix IV (Pro69−Val72) displays a relatively high backbone mobility compared with the other secondary structure elements (see below), none of the residues in the above-mentioned region displays such a pronounced difference in mobility between the two oxidation states of cyt $c_{552}$ as observed for Gly82.

In contrast to the residues displaying significantly decreased order parameter values, most of the secondary structure elements appear to be less mobile (see Figure 4). This is most evident for helices I, III, and V, with average $S^2$ values of (0.89 ± 0.02/0.91 ± 0.03), (0.90 ± 0.03/0.93 ± 0.02), and (0.90 ± 0.02/0.92 ± 0.01) for reduced/oxidized cyt $c_{552}$, respectively. In addition, helix II (red.: 0.88 ± 0.02/ox.: 0.90 ± 0.02) as well as the two concatenated $\beta$-turns between Leu30 and Arg36 (red.: 0.91 ± 0.04/ox.: 0.92 ± 0.03) also display above average order parameters. For helix IV, on the other hand, the average $S^2$ value is much lower (red.: 0.83 ± 0.03/ox.: 0.85 ± 0.01), indicating a higher mobility. As can be seen in Figure 5a, the secondary structure elements apparently form a less flexible domain in the protein structure, except for helix II, which is located on the opposite side of the heme cleft, and helix IV, which appears to be more mobile.

Finally, the additional exchange terms are relatively small ($R_{ex} < 1.5\ s^{-1}$) in both reduced and oxidized cyt $c_{552}$ and show no significant correlation to either dynamic or structural properties of the protein. Consequently, the faster hydrogen exchange observed for the oxidized state relative to reduced cyt $c_{552}$, as described in the following section, apparently is not indicated by the dynamic parameters of the protein backbone.

*Hydrogen Exchange of Amide Protons.* TOCSY spectra of both reduced and oxidized cyt $c_{552}$ were recorded at different times after redissolving the lyophilized protein in $D_2O$. After 1.5 h at 298 K, 44 and 46 slow-exchanging backbone amide protons, belonging mainly to residues located in the α-helices and in the region ranging from Leu30 to Val41, were found in the reduced and oxidized protein samples, respectively. In fact, 40 of these residues were the same for both oxidation states (Figure 5b). After 44.5 h, 34 backbone amide proton resonances were still observed in the reduced protein, while only 14 slow-exchanging amide

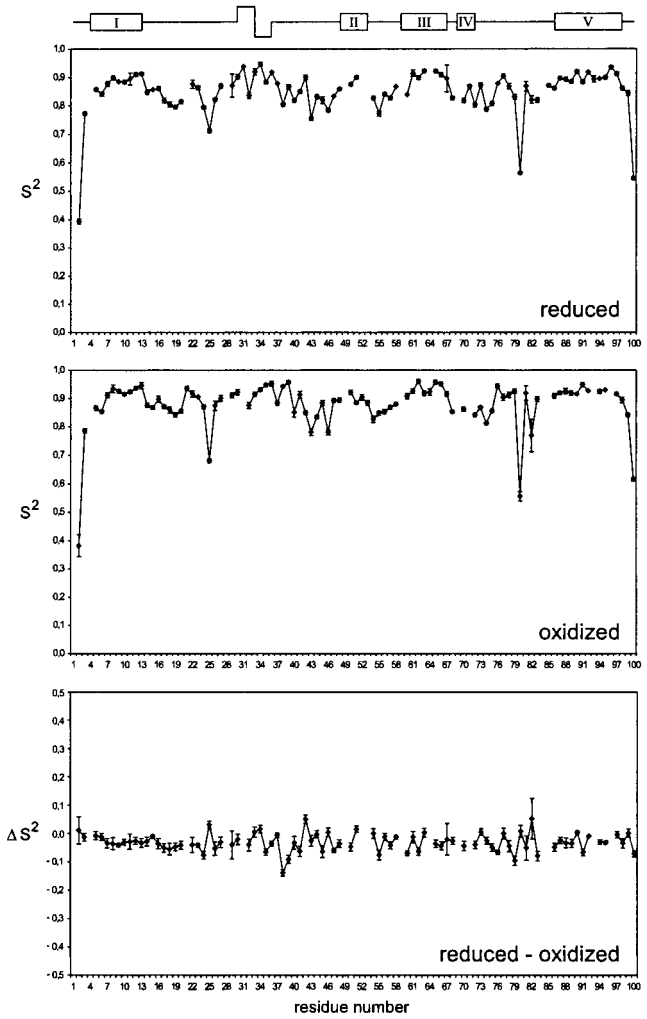


FIGURE 4: Line plots showing the order parameter ($S^2$) values obtained from the complete $^{15}N$ relaxation data at 500 and 600 MHz for reduced (top panel) and oxidized (center panel) cyt $c_{552}$ as well as the difference between the two (bottom panel). Especially pronounced are the low $S^2$ values of Gly25 and Phe80 in both oxidation states. Of further interest is the backbone amide group of Gly82, which displays a significantly higher flexibility in the oxidized cyt $c_{552}$. The secondary structure elements are indicated on top; the helices are labeled with Roman numerals, and the two concatenated $\beta$-turns are represented by the meander motif.

protons remained detectable in the oxidized sample. After 8 days, several amide proton resonances belonging mainly to helices I, II, III, and V as well as Arg36 and Val38 remained visible in the reduced protein, while the signals of the exchangeable protons had basically all disappeared in the oxidized sample. Thus, these results are analogous to data reported by Banci et al. (*7*), where the hydrogen exchange also proceeded much faster in the oxidized cytochrome relative to the reduced protein.

A comparison of the hydrogen exchange data with the $^{15}N$ relaxation data showed that many backbone amide groups with slow-exchanging protons also display increased order parameters and are therefore located in the less flexible parts of the protein. This inverse relationship between slow hydrogen exchange and low order parameters is visualized in Figure 5, where the less flexible protein domain exhibits an increased number of slow-exchanging amide groups. Nevertheless, as mentioned above, the striking differences in the amide proton exchange behavior between reduced and oxidized cyt $c_{552}$ are not at all apparent in the backbone dynamic parameters. Thus, it may be speculated that the differences in structural stability between the two redox states are based on processes that are slow relative to the NMR time scale. Of course, a quantitative determination of hydrogen exchange rates (*39*) in both redox states might elucidate the motional events that lead to the differences in hydrogen exchange.

*Thermostability of Cyt $c_{552}$.* Using differential scanning calorimetry (DSC), a significant difference in the transition temperature ($T_m$) was observed between reduced and oxidized cyt $c_{552}$. While the reduced protein is quite stable up to $T_m = 349.9$ K (76.8 °C), the protein in the oxidized state already unfolds at $T_m = 307.5$ K (34.4 °C), as shown in Figure 6. The molar heat capacity functions of both redox states are not dependent on either protein concentration or heating rate. The denaturation, as monitored by rescanning experiments, is at least partially reversible. The large difference in transition temperatures ($\Delta T_m = 42.4$ K) is in agreement with the temperature-dependent behavior observed in optical spectra (unpublished data) as well as by NMR.

NMR spectra at different temperatures were collected by stepwise heating of the cyt $c_{552}$ protein samples in both redox states, starting at 298 K. Again the reduced protein turned out to be more stable under these conditions. TOCSY and NOESY spectra of reduced cyt $c_{552}$ revealed mostly temperature-dependent chemical shift changes without any indication of protein denaturation up to 338 K, where the temperature series had to be terminated for technical reasons. The NMR spectra of the oxidized protein, however, already showed a transition from predominantly native species to predominantly denatured species at 314 K. Nevertheless, signals belonging to the native oxidized cyt $c_{552}$ showed a continuous decay of intensity up to 323 K, at which point the native species finally disappeared. This rather broad transition corresponds to the DSC data, where the molar heat capacity function starts to decrease at temperatures above 310 K and continues to decline beyond 320 K.

Of particular interest is the temperature-dependent behavior of the aromatic ring proton resonances of the neighboring residues Phe44 and Tyr46. Both residues are located in one corner of the entrance to the heme cleft. The phenol ring of Tyr46 apparently has a slow ring flip rate on the chemical shift time scale, as the pairs of C$\delta$ and C$\epsilon$ protons display separate signals (H$\delta$1 at 8.27/6.97, H$\delta$2 at 7.61/7.19, H$\epsilon$1 at 7.04/5.42, and H$\epsilon$2 at 7.47/7.07 ppm for reduced/oxidized cyt $c_{552}$, respectively). In addition, the O$\eta$H hydroxyl proton resonance is observed at 10.27 ppm (red.) and 9.34 ppm (ox.), indicating a slow exchange due to stable hydrogen bonding to the heme propionate D. In the case of Phe44, on the other hand, only three ring proton resonances (H$\delta$, H$\epsilon$, and H$\zeta$) are present due to a faster ring flip rate. The aromatic proton resonances of both these residues display unusual line-broadening with increased temperature. Phe44 already shows very broad signals at 298 K in both oxidation states, Tyr46 only at higher temperatures. The signals continuously broaden with increasing temperature, until they finally become undetectable. In the reduced cyt $c_{552}$, the Phe44 resonances have disappeared completely at 338 K—more than 10 K below the transition temperature. At the same point, the Tyr46 H$\delta$ and H$\epsilon$ signals are extremely broad and faint in the 2D spectra, and the hydroxyl proton resonance has

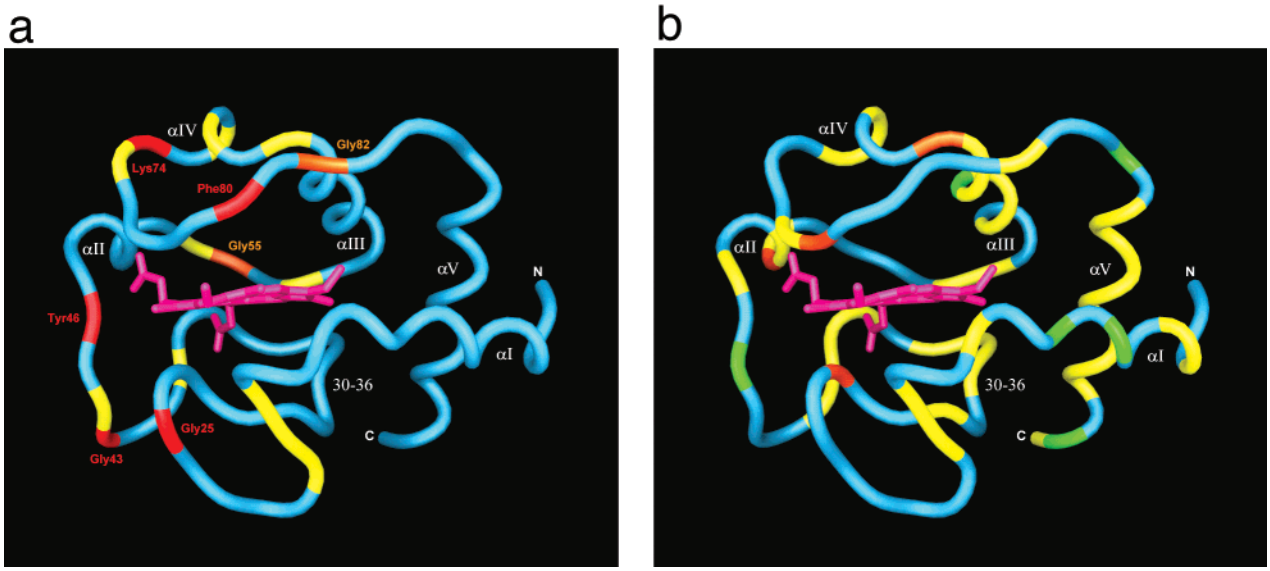


FIGURE 5: (a) Backbone dynamics of cyt $c_{552}$. Aside from the N- and the C-terminus, only residues Gly25, Gly43, Tyr46, Lys74, and Phe80 (all in red with label) show considerably decreased $S^2$ values in both oxidation states, thus indicating higher backbone flexibility. Other residues with below average order parameters in both oxidation states are represented in yellow. The borderline cases Gly55 and Gly82 are displayed in orange. Apparently, the more flexible sections of the protein backbone are located around the heme moiety, while the α-helices I, III, and V together with the two concatenated $\beta$-turns between Leu30 and Arg36 form a less flexible protein domain. (b) Hydrogen exchange in cyt $c_{552}$. Slow-exchanging backbone amide protons, that were observed in the NMR spectra 1.5 h after the exchange reaction was started, are indicated in yellow (for both oxidation states), orange (for reduced state only), or green (for oxidized state only). Clearly, the less flexible regions mentioned above (panel a) exhibit a larger number of slow-exchanging amide protons, suggesting a direct correlation between the backbone dynamic data and the hydrogen exchange behavior [produced with GRASP (*38*)].

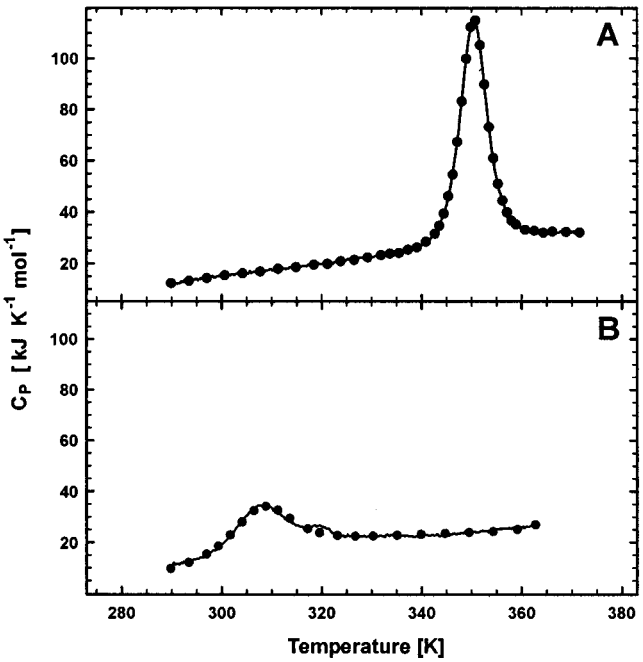


FIGURE 6: Melting curves of cyt $c_{552}$ from DSC measurements. The molar heat capacity functions, $C_p(T)$, of the reduced (panel A) and oxidized (panel B) protein samples are compared. In each case, the experimentally obtained functions are displayed as solid lines, while the dotted lines represent the results of nonlinear fitting in approximation of monomolecular two-state transitions (*native* ↔ *denatured*). The difference in transition temperature between reduced ($T_m$ = 349.9 K) and oxidized ($T_m$ = 307.5 K) cyt $c_{552}$ amounts to $\Delta T_m$ = 42.4 K.

almost completely vanished as well. In the oxidized protein sample, the same effect occurs at lower temperatures: the Phe44 signals are already gone at 303 K, while the Tyr46 signals can be detected as long as the native species is observed (312 K).

The reason for this peculiar behavior of the aromatic proton resonances of Phe44 and Tyr46 may be slow dynamic processes such as conformational exchange, or possibly even signs of initial steps of protein unfolding. The fact that the loop containing Phe44 and Tyr46 apparently belongs to the more flexible region in the cyt $c_{552}$ backbone (see Figure 5a) may be an indication of such an intrinsic property. Certainly, none of the other aromatic rings except Phe65 showed a comparable behavior. In the case of Phe65, however, the line-broadening of the ring resonances decreases with increasing temperature in both oxidation states and therefore can be ascribed to restricted motion of the completely buried phenyl ring (see Figure 2).

After returning the samples to 298 K, the NMR spectrum of reduced cyt $c_{552}$ was identical to the original spectrum before heating, thus indicating that the protein structure had been retained. This is not particularly surprising since this sample was kept far below the transition temperature. In the oxidized sample, however, which had been heated beyond the transition temperature until the native protein species had completely disappeared, about 10% of refolded native protein was found after stepwise cooling to 298 K. This result is in good agreement with the above-described DSC experiments.

The drastically lower thermostability of the oxidized protein state is most probably related to the faster exchange of amide protons relative to reduced cyt $c_{552}$. This difference in thermostability between the reduced and oxidized protein states is of particular interest, since apparently there is no reasonable explanation for such a behavior based on the structural or dynamic data presented above. Both redox states of the native cyt $c_{552}$ appear to be basically identical in terms of molecular interactions such as hydrogen bonds, van der Waals contacts, and salt bridges, except for the charge at

the iron atom. This electrostatic difference apparently is reflected in the two separate fluorescence signals of the nearby tryptophan residue, Trp57, in the reduced (350 nm) and oxidized (330 nm) cyt $c_{552}$ at 298 K (data not shown). Still the question remains whether the difference of a single electron is sufficient to explain the distinct stabilities observed for reduced and oxidized cyt $c_{552}$ by hydrogen exchange and thermodynamic studies. Apparently, these differences in the protein stability emerge only on a relatively slow time scale. Comparative computer simulations of other reduced and oxidized cytochrome systems, e.g., for *Saccharomyces cerevisae* iso-1-cytochrome *c* (*40*), showed that the internal mobility is similar for the two oxidation states over long trajectories although the oxidized form shows greater flexibility in experiment (*7*). Consequently, much longer simulation times may be necessary. However, processes at time scales greater than microseconds are not amenable to molecular simulations at this time; furthermore, the parametrization of the heme in the classical force fields requires improvement, as shown in recent theoretical studies of cytochrome $c_3$ (*41*).

A key to possibly explain the significantly altered stabilities between reduced and oxidized cyt $c_{552}$ could be a comparison of the denatured rather than the native protein structures. The heat denaturation of the oxidized cyt $c_{552}$ might be incomplete and a so-called "partially folded" state formed, thus affecting the total $\Delta G$ value. Earlier folding studies on cytochrome *c* using guanidine hydrochloride have indicated that the protein is more stable toward unfolding in the reduced state (*42*). More elaborate microcalorimetry and hydrogen exchange studies might eventually lead to a better understanding of the unfolding events that govern protein stability on a global, subglobal, and local level (*43*, *44*). It should be noted, however, that the differences in stabilities observed here for the soluble fragment of cytochrome $c_{552}$ may actually be less pronounced for the uncleaved protein in its biological environment.

*Aromatic Rings Important for Electron Transfer*. Surrounding the heme ring are several conserved aromatic residues (Phe11, Phe44, Tyr46, Trp57, Phe65, Phe80, and Tyr95) that could play a role in the redox reaction (see Figure 2). In particular, the phenyl rings of Phe44 and Phe80 are both solvent-accessible and located in opposite corners of the entrance to the heme cleft. The highly conserved Phe80 (corresponding to Phe82 of horse heart cytochrome *c*) is believed to play an important role in the biological function of cytochrome *c* (*45*), which is supported by the fact that in cyt $c_{552}$ it may not be replaced by a nonaromatic residue without complete loss of ET activity (V. Drosou, unpublished data). The aromatic ring of Phe80 is close to the iron atom (6.9 Å from the ring center), oriented nearly parallel to the heme plane. In the X-ray study on cyt $c_{552}$ (*9*), small movements of the Phe80 ring were detected in two of the four cytochrome molecules in the asymmetric unit upon change of oxidation state. Although moderate redox-induced shifts of the ring proton resonances are observed in solution, the position of the Phe80 ring is basically the same in all NMR structures. Interestingly though, the backbone amide group of this residue (together with Gly82 in oxidized cyt $c_{552}$) shows unusually low order parameters in both oxidation states, which could be related to increased backbone mobility in this region.

Another aromatic ring close to the heme iron belongs to Phe65 (6.9 Å from the ring center), which in cyt $c_{552}$ may also not be mutated to a nonaromatic residue without loss of ET capability (V. Drosou, unpublished data). This residue is completely buried in the interior of the protein structure as mentioned above. It is positioned nearly perpendicular to the heme plane and located within the region of influence of the paramagnetic iron. Therefore, the ring proton resonances of Phe65 in the oxidized state are strongly shifted relative to the reduced state by +1.74, +6.43, and +10.14 ppm for H$\delta$, H$\epsilon$, and H$\zeta$, respectively. Phe65 corresponds to Tyr67 in horse heart cytochrome *c*, which together with Asn52 and Thr78 forms a hydrogen bond network with the second conserved internal water molecule (number 112 in eukaryotic *c*-type cytochromes). In the case of horse heart cytochrome *c*, small movements of this internal water molecule as well as the induction of further molecular movements in the immediate vicinity have been observed between the two oxidation states and were subsequently discussed to play a possible role in the mechanism of eukaryotic *c*-type cytochromes (*10*, *11*, *46*, *47*). In cytochrome $c_{552}$ from *P. denitrificans*, however, this particular water molecule is absent (*9*), the phenyl ring of Phe65 is incapable of hydrogen bond formation, and Asn52 is replaced by Met50. Therefore, the data obtained for this prokaryotic member of the cytochrome *c* family suggest a different mechanistic situation.

The extreme line-broadening effects observed for the Phe44 and Tyr46 ring proton resonances have already been discussed above in detail. In mitochondrial *c*-type cytochromes, the position of Phe44 is occupied either by a tyrosine or by a phenylalanine residue, while Tyr46 is highly conserved. The positions of these aromatic rings are comparable in all NMR and X-ray structures of cyt $c_{552}$. The functional roles of Phe44 and Tyr46 are certainly not understood at present, but the unusual effects observed by NMR and their prominent positions at the entrance to the heme cleft suggest that these two residues may in some way be involved either in the ET process or in protein folding and stability. Certainly, site-directed mutations of these residues will prove to be helpful tools to further elucidate this question.

## CONCLUSIONS

A biologically fully active 10.5 kDa fragment of the *P. denitrificans* cytochrome $c_{552}$ enriched with $^{13}C$ and $^{15}N$ isotopes has been prepared for high-resolution NMR studies. The solution structures of the reduced and oxidized states were obtained through NOE-derived distance information. The overall fold resembles that seen throughout the *c*-type cytochrome family, consisting of two long terminal helices and three shorter helices surrounding the heme moiety.

No significant redox-induced differences could be observed for cyt $c_{552}$ with regard to either the structural fold or the backbone dynamics within the picosecond−nanosecond time scale. In both oxidation states, the protein is divided into a more flexible backbone domain surrounding the heme moiety and a less mobile domain including the α-helices I, III, and V as well as the two concatenated $\beta$-turns between Leu30 and Arg36. Nevertheless, certain distinctions must exist between the two redox states, as indicated by the

remarkable differences in hydrogen exchange and thermostability. The oxidized protein state is much less stable compared to reduced cyt $c_{552}$, displaying a considerably lower transition temperature and much faster exchange of backbone amide protons.

Of particular interest are the aromatic residues Phe44, Tyr46, and Phe80, which are located at the entrance to the heme cleft and exhibit rather unusual effects in the NMR data, as well as Trp57 and Phe65, which are buried inside the protein close to the heme moiety. Their precise functional roles in the redox processes with other ET partners remain an interesting goal for further investigations.

## ACKNOWLEDGMENT

We thank Ingrid Weber (University of Frankfurt, Germany) for assistance in the preparative work, as well as Prof. Lucia Banci and Dr. Antonio Rosato (University of Florence, Italy) for their valuable help with the programs FANTASIA and PSEUDYANA.

## SUPPORTING INFORMATION AVAILABLE

Tables of $^{15}N$ relaxation data obtained for reduced and oxidized cyt $c_{552}$ (6 pages). This information is available free of charge via the Internet at http://pubs.acs.org.

## REFERENCES

1. Moore, G. R., and Pettigrew, G. W. (1990) in *Cytochromes c; Evolutionary, Structural and Physicochemical Aspects*, Springer-Verlag, Berlin.
2. Scott, R. A., and Mauk, A. G. (1996) in *Cytochrome c—A multidisciplinary approach*, University Science Books, Sausalito, CA.
3. Berry, E. A., and Trumpower, B. L. (1985) *J. Biol. Chem. 260*, 2458−2467.
4. Turba, A., Jetzek, M., and Ludwig, B. (1995) *Eur. J. Biochem. 231*, 259−265.
5. Reincke, B., Thöny-Meyer, L., Dannehl, C., Odenwald, A., Aidim, M., Witt, H., Rüterjans, H., and Ludwig, B. (1999) *Biochim. Biophys. Acta 1441*, 114−120.
6. Pristovšek, P., Lücke, C., Reincke, B., Ludwig, B., and Rüterjans, H. (2000) *Eur. J. Biochem. 267*, 4205−4212.
7. Banci, L., Bertini, I., Bren, K. L., Gray, H. B., Sompornpisut, P., and Turano, P. (1997) *Biochemistry 36*, 8992−9001.
8. Fetrow, J. S., and Baxter, S. M. (1999) *Biochemistry 38*, 4480−4492.
9. Harrenga, A., Reincke, B., Rüterjans, H., Ludwig, B., and Michel, H. (2000) *J. Mol. Biol. 295*, 667−678.
10. Takano, T., and Dickerson, R. E. (1981) *J. Mol. Biol. 153*, 79−94.
11. Takano, T., and Dickerson, R. E. (1981) *J. Mol. Biol. 153*, 95−115.
12. Berghius, A. M., and Brayer, G. D. (1992) *J. Mol. Biol. 214*, 585−595.
13. Qi, P. X., Beckmann, R. A., and Wand, A. J. (1996) *Biochemistry 35*, 12275−12286.
14. Pristovšek, P., Lücke, C., Reincke, B., Löhr, F., Ludwig, B., and Rüterjans, H. (2000) *J. Biomol. NMR 16*, 353−354.
15. Kay, L. E., Keifer, P., and Saarinen, T. (1992) *J. Am. Chem. Soc. 114*, 10663−10665.
16. Schleucher, J., Sattler, M., and Griesinger, C. (1993) *Angew. Chem., Int. Ed. Engl. 32*, 1489−1491.
17. Kay, L. E., Marion, D., and Bax, A. (1989) *J. Magn. Reson. 84*, 72−84.
18. Zuiderweg, E. R. P., and Fesik, S. W. (1989) *Biochemistry 28*, 2387−2391.
19. Lücke, C., Reincke, B., Löhr, F., Pristovšek, P., Ludwig, B., and Rüterjans, H. (2000) *J. Biomol. NMR 18*, 365−366.
20. Peng, J., and Wagner, G. (1992) *J. Magn. Reson. 98*, 308−332.
21. Peng, J., and Wagner, G. (1992) *Biochemistry 31*, 8571−8586.
22. Cavanagh, J., Fairbrother, W. J., Palmer, A. G., III, and Skelton, N. J. (1996) in *Protein NMR spectroscopy—principles and practice*, Academic Press, San Diego, CA.
23. Mandel, A. M., Akke, M., and Palmer, A. G. (1995) *J. Mol. Biol. 246*, 144−163.
24. Palmer, A. G., Rance, M., and Wright P. E. (1991) *J. Am. Chem. Soc. 113*, 4371−4380.
25. La Mar, G. N., and de Ropp, J. S. (1993) in *NMR of paramagnetic molecules* (Berliner, L. J., and Reuben, J., Eds.) pp 1−78, Plenum Press, New York.
26. Filimonov, V. V., and Rogov, V. V. (1996) *J. Mol. Biol. 255*, 767−777.
27. Güntert, P., Braun, W., and Wüthrich, K. (1991) *J. Mol. Biol. 217*, 517−530.
28. Wüthrich, K. (1986) in *NMR of proteins and nucleic acids*, Wiley, New York.
29. Güntert, P., Mumenthaler, C., and Wüthrich, K. (1997) *J. Mol. Biol. 273*, 283−298.
30. Banci, L., Bertini, I., Gray, H. B., Luchinat, C., Reddig, T., Rosato, A., and Turano, P. J. (1997) *Biochemistry 36*, 9867−9877.
31. Banci, L., Bertini, I., Cremonini, M. A., Gori-Savellini, G., Luchinat, C., Wüthrich, K., and Güntert, P. (1998) *J. Biomol. NMR 12*, 553−557.
32. Banci, L., Bertini, I., Bren, K. L., Cremonini, M. A., Gray, H. B., Luchinat, C., and Turano, P. (1996) *J. Biol. Inorg. Chem. 1*, 117−126.
33. Banci, L., Bertini, I., Gori Savellini, G., Romagnoli, A., Turano, P., Cremonini, M. A., Luchinat C., and Gray, H. B. (1997) *Proteins: Struct., Funct., Genet. 29*, 68−76.
34. Laskowski, R. A., MacArthur, M. W., Moss, D. S., and Thornton, J. M. (1993) *J. Appl. Crystallogr. 26*, 283−291.
35. Kraulis, P. J. (1991) *J. Appl. Crystallogr. 24*, 946−950.
36. Merritt, E. A., and Bacon, D. J. (1997) *Methods Enzymol. 277*, 505−524.
37. Banci, L., Bertini, I., Huber, J. G., Luchinat, C., and Rosato, A. (1998) *J. Am. Chem. Soc. 120*, 12903−12909.
38. Nicholls, A., Sharp, K. A., and Honig, B. (1991) *Proteins: Struct., Funct., Genet. 11*, 281−296.
39. Milne, J. S., Mayne, L., Roder, H., Wand, A. J., and Englander, S. W. (1998) *Protein Sci. 7*, 739−745.
40. Banci, L, Gori-Savellini G., and Turano, P. (1997) *Eur. J. Biochem. 249*, 716−723.
41. Soares, C. M., Martel, P. J., Mendes, J., and Carrondo, M. A. (1998) *Biophys. J. 74*, 1708−1721.
42. Pascher, T., Chesick, J. P., Winkler, J. R., and Gray, H. B. (1996) *Science 271*, 1558−1560.
43. Sadqi, M., Casares, S., Abril, M. A., López-Mayorga, O., Conejero-Lara, F., and Freire, E. (1999) *Biochemistry 38*, 8899−8906.
44. Bai, Y., Sosnick, T. R., Mayne, L., and Englander, S. W. (1995) *Science 269*, 192−197.
45. Liang, N., Mauk, A. G., Pielak, G. J., Johnson, J. A., Smith, M., and Hoffman, B. M. (1988) *Science 240*, 311−313.
46. Bushnell, G. W., Louie, G. V., and Brayer, G. D. (1990) *J. Mol. Biol. 214*, 905−921.
47. Qi, P. X., Urbauer, J. L., Fuentes, E. J., Leopold, M. F., and Wand, A. J. (1994) *Nat. Struct. Biol. 1*, 378−382.

BI010615O